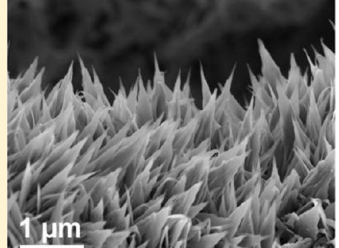


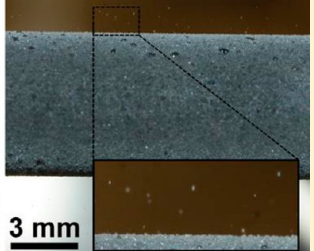
Jumping-Droplet-Enhanced Condensation on Scalable Superhydrophobic Nanostructured Surfaces

Nenad Miljkovic,[†] Ryan Enright,^{†,‡,||} Youngsuk Nam,^{†,§} Ken Lopez,[†] Nicholas Dou,[†] Jean Sack,[†] and Evelyn N. Wang*,[†]

Supporting Information

ABSTRACT: When droplets coalesce on a superhydrophobic nanostructured surface, the resulting droplet can jump from the surface due to the release of excess surface energy. If designed properly, these superhydrophobic nanostructured surfaces can not only allow for easy droplet removal at micrometric length scales during condensation but also promise to enhance heat transfer performance. However, the rationale for the design of an ideal nanostructured surface as well as heat transfer experiments demonstrating the advantage of this jumping behavior are lacking. Here, we show that





silanized copper oxide surfaces created via a simple fabrication method can achieve highly efficient jumping-droplet condensation heat transfer. We experimentally demonstrated a 25% higher overall heat flux and 30% higher condensation heat transfer coefficient compared to state-of-the-art hydrophobic condensing surfaces at low supersaturations (<1.12). This work not only shows significant condensation heat transfer enhancement but also promises a low cost and scalable approach to increase efficiency for applications such as atmospheric water harvesting and dehumidification. Furthermore, the results offer insights and an avenue to achieve high flux superhydrophobic condensation.

KEYWORDS: Jumping droplets, nanostructure, superhydrophobic surface, enhanced condensation, condensation heat transfer

ondensation is a ubiquitous phase-change process that is an essential natural phenomenon and widely used in various industries. Enhancement of condensation heat and mass transfer promises considerable savings in energy and natural resources for applications including water harvesting, 1,2 desalination,3 thermal management,4 industrial power generation,5 and building heating and cooling.6,7 As a result, dropwise condensation with nonwetting substrates has attracted much attention since its discovery by Schmidt et al. in the early 1930s due to the potential for higher phase-change heat transfer performance when compared to filmwise condensation. 8,9 To achieve efficient dropwise condensation, however, condensate droplets must be rapidly removed from the surface because the increasing droplet size acts as a thermal barrier. 10 For traditional dropwise condensing surfaces, such a removal typically relies on gravity, where droplet sizes have to approach the capillary length (\approx 2.7 mm for water) to overcome the contact line pinning force. 11,12

A recent study on structured superhydrophobic surfaces, however, demonstrated that, when small droplets ($\approx 10-100$ μ m) merge on suitably designed superhydrophobic surfaces, they can undergo coalescence-induced droplet ejection or "jumping" independent of gravity 13 due to the release of excess

surface energy. The nanostructured surface beneath the coalescing droplets reduces the droplet adhesion to the substrate by minimizing the solid fraction¹⁴ and breaks the symmetry of the coalesced droplet. 13 As a result, the droplet accelerates and departs perpendicular to the surface. Such droplet jumping offers an avenue to further enhance condensation heat transfer over conventional dropwise condensation by increasing the time-averaged density of small droplets, which transfer heat more efficiently from the vapor to the substrate. 15-19 While a considerable amount of work has focused on understanding and fabricating structured surfaces to sustain droplet jumping, ^{13,15–18,20–27} heat transfer measurements that quantify the amount of enhancement possible using these surfaces are lacking. In addition, past studies have utilized surfaces that are relatively expensive to fabricate, typically require the use of a cleanroom environment and generally are not applicable to arbitrarily shaped surfaces, which presents challenges in the eventual scale-up for large scale thermal applications.

Received: October 16, 2012 Revised: November 16, 2012 Published: November 28, 2012

Department of Mechanical Engineering, Massachusetts Institute of Technology, 77 Massachusetts Avenue, Cambridge, Massachusetts 02139, United States

^{*}Stokes Institute, University of Limerick, Limerick, Ireland

[§]Kyung Hee University, Yongin, Korea

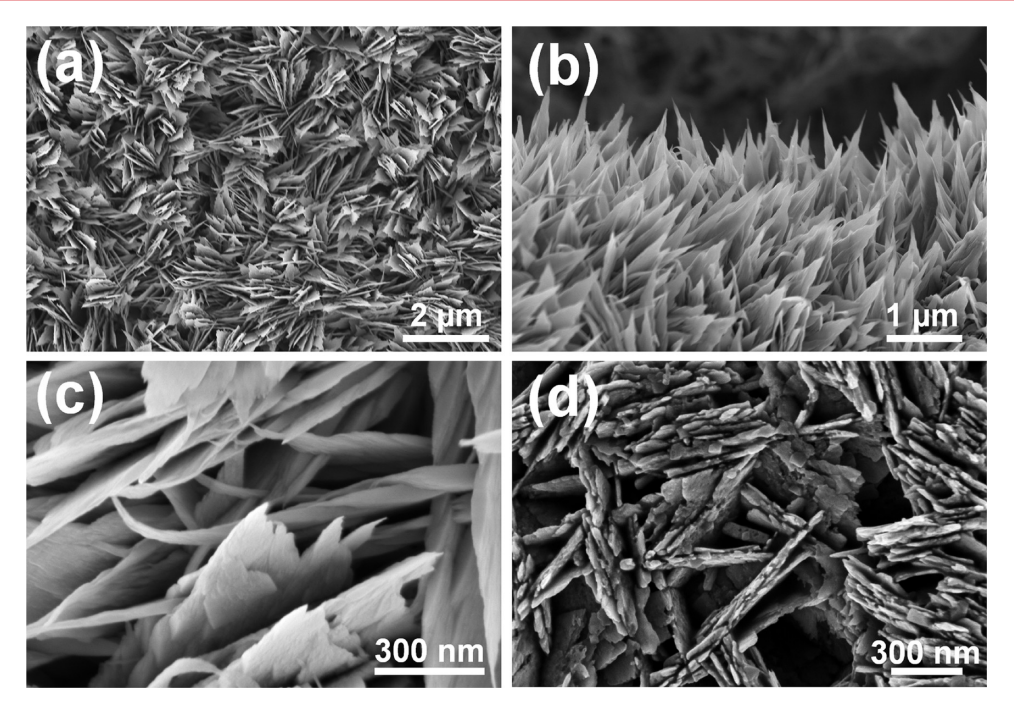


Figure 1. Nanostructure characterization. Field emission scanning electron microscopy (FESEM) images of a 5 min CuO surface with (a) top view, no silane, (b) side view, no silane, (c) high magnification showing the blade structure of the oxide, no silane, and (d) high magnification after silane deposition. Due to imperfect monolayer formation, silane deposition thickens the oxide blades but maintains the general nanostructure morphology. The sharp, knife-like CuO structures have characteristic heights, $h \approx 1~\mu\text{m}$, solid fraction, $\phi \approx 0.023$, and roughness factor, $r \approx 10$.

In this work, we experimentally demonstrated that a 25% higher overall heat flux and 30% higher condensation heat transfer coefficient can be achieved using silanized copper oxide (CuO) superhydrophobic surfaces compared to conventional dropwise condensing copper (Cu) surfaces at low supersaturations (S < 1.12). We show that these CuO surfaces offer ideal condensation behavior in terms of emergent droplet morphology and coalescence dynamics and a significant enhancement in heat transfer performance when compared to state-of-the-art condensing surfaces. Furthermore, the chemicaloxidation-based CuO fabrication process provides a simple and readily scalable method to create superhydrophobic condensation surfaces that can sustain droplet jumping behavior. Accordingly, these surfaces are attractive for applications such as atmospheric water harvesting and dehumidification where the heat fluxes are relatively low and droplets can be maintained in a highly mobile state.

We investigated the heat transfer behavior of Cu tubes, which are representative of a typical heat exchanger geometry and material, 28,29 coated with functionalized CuO nanostructures. Figure 1a, b, and c show top, side, and high resolution images of the CuO nanostructures, respectively. Chemical-oxidationbased CuO nanostructuring was chosen as the ideal fabrication method due to its self-limiting growth behavior and low characteristic oxide thickness ($h \approx 1 \mu m$, Figure 1b), promising a low parasitic conduction thermal resistance ($k_{\text{CuO}} \approx 20 \text{ W}/$ m·K).³⁰ In addition, the knife-like nanostructure features (\leq 10 nm, Figure 1c) ensure nucleation within the structure (as opposed to the tips of the structure) due to the increased energy barrier associated with nucleation on features similar in size to the critical nucleation radius ($r_c \le 35$ nm for water and typical conditions). Therefore, the formation of partially wetting droplet morphologies, which are essential to minimizing individual droplet thermal resistance, ^{18,31} are favored since Gibb's criterion can be satisfied. ^{32,33} Furthermore, the small characteristic length scale of the nanostructure spacing (\approx 1 μ m, Figure 1a) allows for higher nucleation densities, and thus higher supersaturations prior to surface flooding, typically seen on larger scale microstructured surfaces. From an industrial perspective, this fabrication method has several additional advantages: (i) it can be applied to arbitrarily shaped surfaces, (ii) the nanostructures can be formed over large areas, (iii) the nanostructures form at low temperatures and do not require any high temperature annealing or drying processes, and (iv) the oxide growth mechanism is self-limiting, creating a uniform and thin nanostructure layer independent of oxidation time. Once the CuO surface is chemically functionalized (Figure 1d, Table 1), coalescence induced droplet jumping is stable and frequent.

Table 1. Sample Wetting Characteristics^a

sample ID	oxidation time, τ (min)	silanization time (min)	advancing angle (deg)	receding angle (deg)
hydrophilic Cu	0	0	14.6 ± 6.6	<3
hydrophobic Cu	0	60	123.4 ± 2.5	81.2 ± 8.4
CuO	5	60	169.2 ± 2.6	164.1 ± 5.2
CuO	10	60	171.2 ± 3.1	167.2 ± 3.2
CuO	20	60	172.3 ± 2.9	168.5 ± 3.1
CuO	45	60	172.0 ± 3.2	167.8 ± 3.2
aa.1	. 1 . 4	/		

"Silane chemistry, tridecafluoro-(1,1,2,2-tetrahydrooctyl)-1-trichlorosilane was used.

We used commercially available oxygen-free Cu tubes (99.9% purity) with outer diameters, $D_{\rm OD}$ = 6.35 mm, inner diameters, $D_{\rm ID}$ = 3.56 mm, and lengths, L = 131 mm as the test samples for the experiments. Each Cu tube was cleaned in an ultrasonic bath with acetone for 10 min and rinsed with ethanol, isopropyl alcohol, and deionized (DI) water. The tubes were then dipped

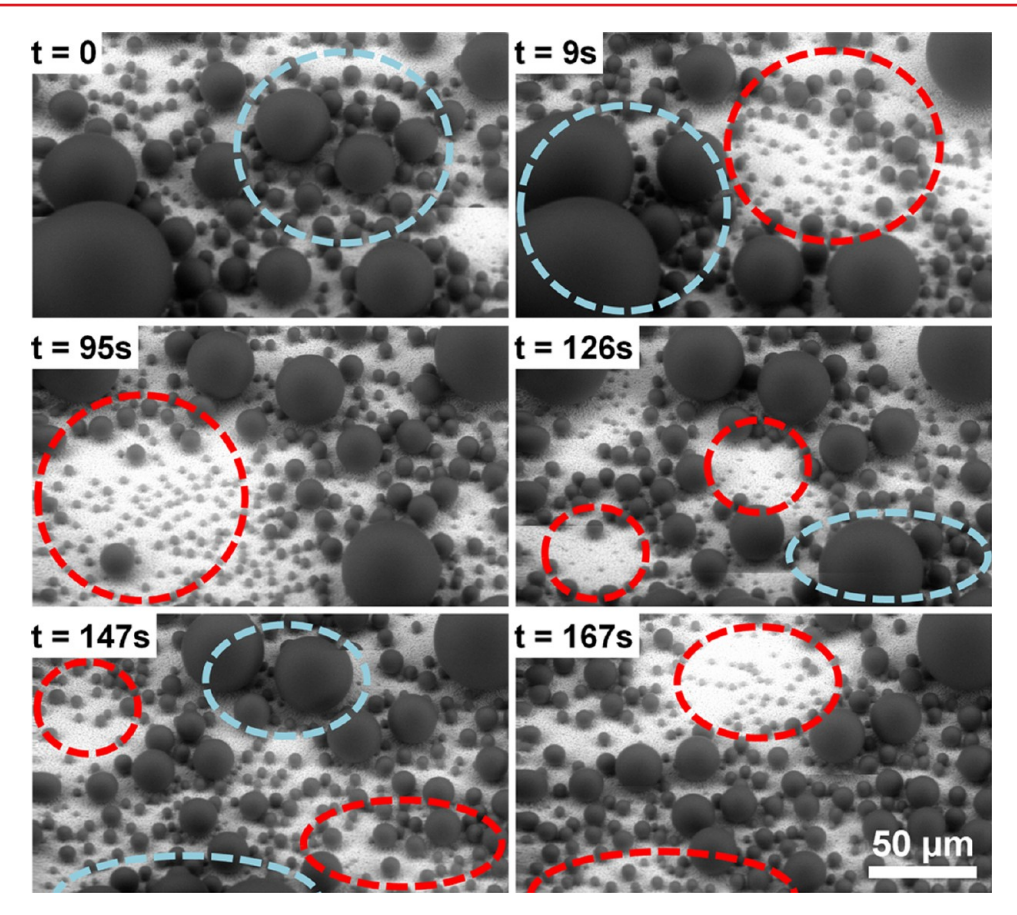


Figure 2. Droplet growth dynamics. Time-lapse images captured via environmental scanning electron microscopy (ESEM) of steady state water condensation on a 10 min CuO surface. A large viewing area was used to avoid electron beam heating effects. Condensing droplets underwent spontaneous droplet jumping and surface renewal. Light blue dotted circles highlight areas of the surface with droplets just prior to coalescence and subsequent jumping, while red dotted circles highlight areas of the surface right after droplet jumping ($P_v = 860 \pm 43 \text{ Pa}$, $T_s = 4.5 \pm 1.5$ °C, S = 1.02, see Supporting Information, video S1).

into a 2.0 M hydrochloric acid solution for 10 min to remove the native oxide film on the surface, then triple-rinsed with DI water, and dried with clean nitrogen gas.

Nanostructured CuO films were formed by immersing the cleaned tubes into a hot (96 \pm 3 °C) alkaline solution composed of NaClO₂, NaOH, Na₃PO₄·12H₂O, and DI water (3.75:5:10:100 wt %). $^{17,34-36}$ During the oxidation process, a thin (\approx 300 nm) Cu₂O layer was formed that then reoxidized to form sharp, knife-like CuO oxide structures with heights of $h\approx$ 1 μ m, solid fraction $\varphi\approx$ 0.023, and roughness factor $r\approx$ 10 (Figure 1a, b, and c, see Supporting Information, section S5). To verify the independence of oxide thickness on chemical oxidation time, four separate samples were made using oxidation times, $\tau=$ 5, 10, 20, and 45 min.

In addition to the nanostructured CuO tubes, we tested smooth Cu tubes silanized to be hydrophobic (dropwise) or plasma cleaned to be hydrophilic (filmwise) for benchmark comparisons. Smooth oxidized Cu surfaces were achieved by immersing the cleaned tubes into a room temperature solution of $\rm H_2O_2$ (hydrogen peroxide, Sigma-Aldrich) for 20 min to form a thin (≈ 300 nm) Cu₂O layer (see Supporting Information, section S5).

Hydrophobic functionalization of both the nanostructured CuO and smooth Cu tubes was obtained by depositing a fluorinated silane (trichloro(1H,1H,2H,2H-perfluorooctyl)-silane, Sigma-Aldrich) in the vapor phase. This self-assembled coating had a typical advancing angle of $\theta_a \approx 120^\circ$ when

measured on a smooth reference surface (Table 1). While the silane deposition step thickens the nanostructures by ≈ 10 nm (due to polycondensation of chlorosilanes),³⁷ the general morphology was left unchanged (Figure 1d).

Individual droplet growth on the nanostructured CuO surfaces was characterized using environmental scanning electron microscopy (ESEM). Figure 2 shows timelapse images of condensation on the nanostructured CuO surface (see Supporting Information, video S1). Droplets nucleated within the nanostructures and, while growing beyond the confines of the structures, their apparent contact angle increased as they developed a balloon-like shape with a liquid bridge at the base. 17 This pinning behavior is consistent with the calculated preferred wetting state $E^* = -1/(r \cdot \cos \theta_a) \approx 0.2$ < 1.²¹ Furthermore, this formation of partially wetting droplets is crucial for maximizing individual droplet growth rates by minimizing the droplet-base thermal resistance.²² Once droplets grew to diameters large enough to coalesce with neighboring droplets ($R \approx 7 \ \mu \text{m}$), frequent out-of-plane jumping droplets were observed. ¹³ In addition to the removal of coalescing droplets, smaller droplets located near the coalescing pair were also removed (Figure 2). This sweeping behavior created by coalescing droplet pairs is attributed to the inertially driven shape change generated during coalescence which can stretch the droplet and result in coalescence with multiple neighboring droplets. 13,47

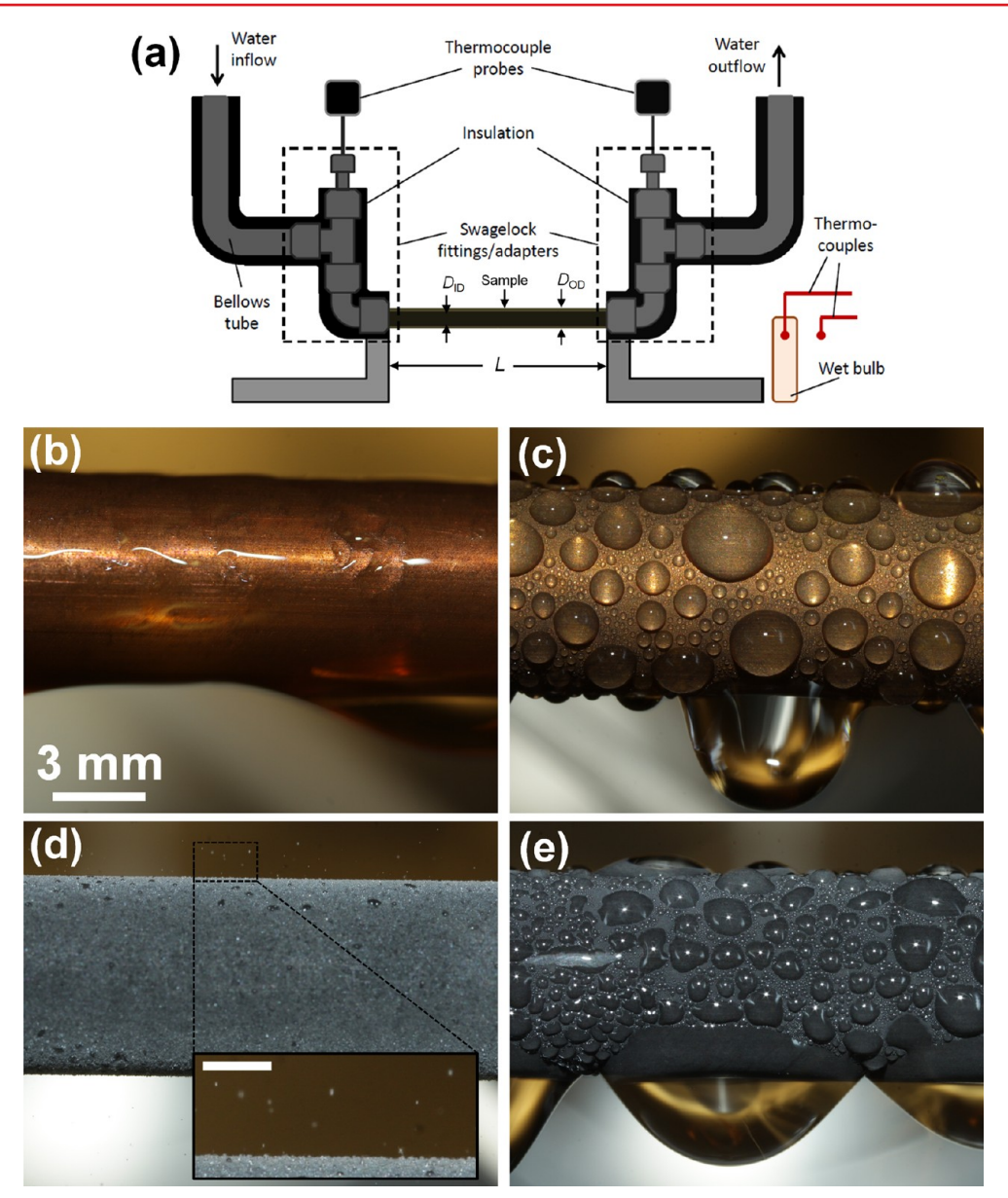


Figure 3. Test setup and experimental images of condensation. (a) Schematic showing experimental setup. The tube sample ($D_{\rm OD}$ = 6.35 mm, $D_{\rm ID}$ = 3.56 mm, L = 131 mm) was cooled via chilled water flowing inside the tube at 5 \pm 0.1 L/min. Images of (b) filmwise condensation on a smooth hydrophilic Cu tube, (c) dropwise condensation on a silane coated smooth Cu tube, (d) jumping-droplet superhydrophobic condensation on a nanostructured CuO tube (10 min oxidation) (inset: magnified view of the jumping phenomena, scale bar is 500 μ m), and (e) flooded condensation on a nanostructured CuO tube. The tube dimensions are identical for each case (chamber vapor pressure $P_{\rm v}$ = 2700 \pm 68 Pa).

To determine the overall condensation heat transfer performance, the CuO nanostructured tubes were tested in a controlled condensation chamber (Supporting Information, section S2). Prior to performing the experiments, the vapor supply of water was vigorously boiled, and the test chamber was evacuated to a pressure $P < 0.5 \pm 0.025$ Pa to eliminate noncondensable gases. Throughout the experiments, the chamber pressure and temperature were continuously monitored to ensure saturated conditions. The temperature of the tube was independently controlled via a cooling loop, and inlet and outlet tube temperatures were measured to determine the condensation heat flux (Figure 3a). The vapor pressure range tested (2 kPa < $P_{\rm v}$ < 3.6 kPa) corresponds to steam saturation temperatures of 17.5–27 °C, which are common conditions for building energy, dehumidification, and high efficiency industrial condenser applications. Typical inlet to outlet tube

temperature differences ranged from 0.5 to 2.5 $^{\circ}\mathrm{C}$ depending on the tube sample and vapor pressure.

Figure 3b shows an image obtained during filmwise condensation on the clean, smooth hydrophilic Cu tube. As expected, vapor condensed and formed a thin liquid film that covered the entire surface (see Supporting Information, video S2). Meanwhile, Figure 3c shows an image during conventional dropwise condensation on the smooth hydrophobic Cu tube where discrete droplets formed and grew to sizes approaching the capillary length (\approx 2.7 mm) before being removed by gravity (see Supporting Information, video S3). The condensation mechanism on both of the smooth Cu tubes (hydrophilic and hydrophobic) was independent of the supersaturation S, defined as the ratio of the vapor pressure to the saturation pressure corresponding to the sample surface temperature ($S = P_v/P_w$). In contrast, condensation on the

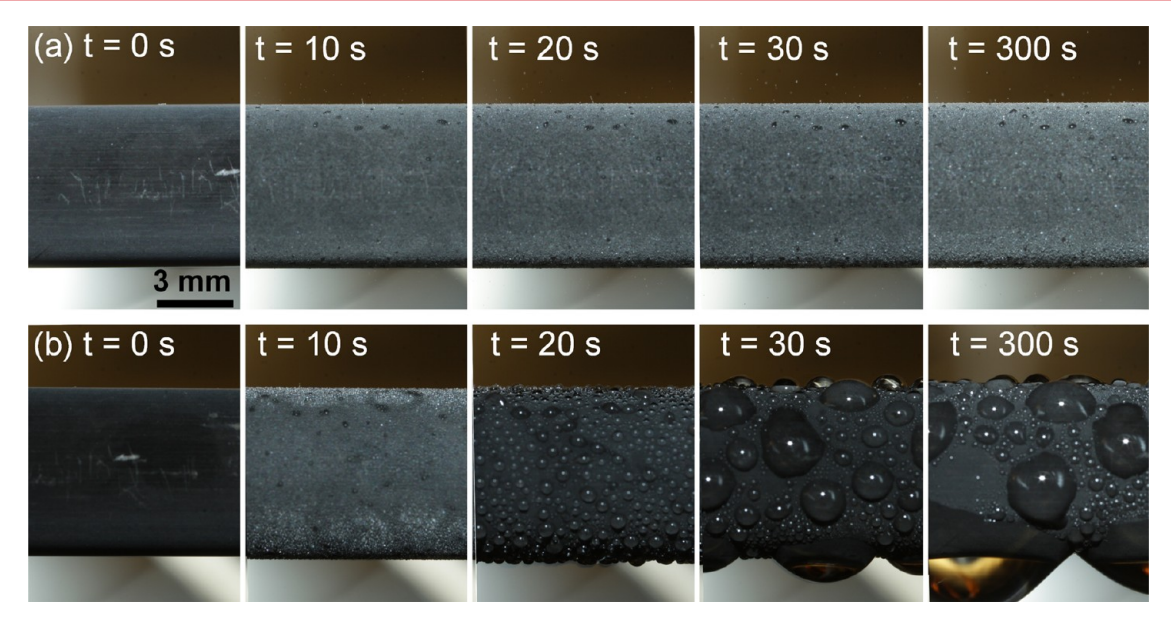


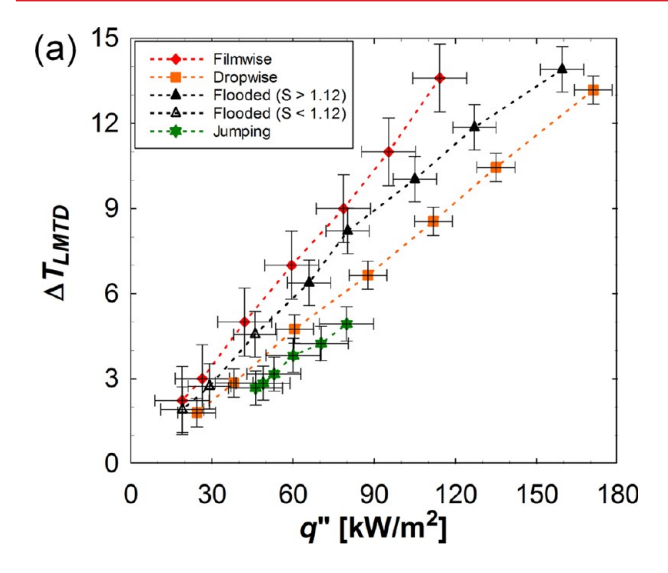
Figure 4. Jumping and flooded condensation. Time-lapse images of initial water condensation on a 10 min oxidized CuO sample undergoing (a) jumping (S = 1.08, $\Delta T_{\rm LMTD} = 4$ K, $P_{\rm v} = 2700 \pm 68$ Pa) and (b) flooded condensation (S = 1.54, $\Delta T_{\rm LMTD} = 12$ K, $P_{\rm v} = 2700 \pm 68$ Pa). Low supersaturations (S = 1.08) led to highly mobile partially wetting droplet formation and subsequent droplet jumping. High supersaturations (S = 1.54) led to surface flooding and the formation of highly pinned Wenzel droplet morphologies.

nanostructured CuO surface showed significant dependence on the supersaturation. Figure 3 parts d and e show images during condensation on the nanostructured CuO surface for low (S =1.08) and high (S = 1.54) supersaturations, respectively (see Supporting Information, videos S4 and S5). At the low supersaturation (Figure 3d), the CuO surface showed very efficient droplet removal via the jumping mechanism, with numerous microscale droplets ($R \approx 8 \mu m$) populating the surface (see Supporting Information, section S5). However, as the supersaturation was increased to 1.54 (by lowering the cooling water temperature), the emergent droplet morphology transitioned from highly mobile jumping droplets to highly pinned Wenzel droplets, which completely wet the cavities of the nanostructure. Figure 4 parts a and b show time-lapse images of the jumping and flooding condensation mechanisms, respectively, during initial transient condensate formation. Note that the transition from jumping to Wenzel droplets on the surface was not reversible, that is, once flooding initiated, reduction of the supersaturation did not revert the behavior to droplet jumping. The only means to recover the droplet jumping mode was to increase the cooling water temperature enough to re-evaporate all of the condensate and then reinitiate condensation at a low supersaturation. This observed hysteresis in the heat transfer behavior indicates that the procedure used to obtain steady operation of the condensing surface is extremely important.

The hysteresis can be explained in terms of the interplay between the characteristic structure length scale and droplet nucleation density. At low supersaturations (S < 1.12, low nucleation density), droplets formed with large spacings between each other relative to the spacing of the nanostructures such that the droplet could evolve into the energetically favorable partially wetting (PW) Cassie-like morphology (Figure 2). For higher supersaturations (S > 1.12), the droplet nucleation density increased to the point where droplet/droplet interactions occurred on a similar length scale as the nanostructure spacing ($\approx 1~\mu m$), and droplets, instead of forming in the energetically favorable PW morphology, merged

to form pinned liquid films due to contact line depinning at their base. Further condensation on the "flooded" surface resulted in the formation of Wenzel droplets which demonstrated significant contact line pinning as evidenced by the large droplet shedding diameters and irregular droplet shapes. It is important to note that the critical radius for droplet nucleation at supersaturation conditions (1.02 < S < 1.2) which include jumping (S < 1.12) and flooding (S > 1.12) was 8 nm (S = 1.2) < r_c < 41 nm (S = 1.02), which is much smaller than the characteristic structure length scale (I ≈ 1 μ m). The length scale discrepancy (I c I I I implies that the flooding transition did not occur due to further reduction in I I as the supersaturation was increased (I > 1.12), since the critical nuclei were already well below the structure length scale.

Figure 5a shows the measured heat flux with the log mean water-to-vapor temperature difference ($\Delta T_{\text{LMTD}} = [(T_{\text{v}} - T_{\text{in}})]$ - $(T_{\rm v}-T_{\rm out})]/{\rm ln}[(T_{\rm v}-T_{\rm in})/(T_{\rm v}-T_{\rm out})]$, where $T_{\rm v}$, $T_{\rm in}$, and $T_{\rm out}$ are the vapor, cooling water inlet, and cooling water outlet temperatures, respectively) as a function of the condensation heat flux (q'') at a vapor pressure $P_v = 2700 \pm 68$ Pa. To maximize the tube internal heat transfer coefficient, the cooling water mass flow rate was held constant at 5 ± 0.1 L/min for all experiments (1.02 < $S \le 1.6$, 10 < $T_s < 25$ °C, where T_s is the extrapolated tube surface temperature, see Supporting Information, section S6). Condensation on the filmwise (diamond symbols) and dropwise (square symbols) Cu surfaces served as baseline cases for comparing condensation performance. The overall heat transfer coefficient (HTC), \bar{U} = $q''/\Delta T_{\rm LMTD}$, was obtained from the slope. As expected, the Cu tube with filmwise behavior showed the worst overall HTC $(\overline{U}_{\text{filmwise}} = 8.92 \pm 1.14 \text{ kW/m}^2 \text{ K})$ due to the thin liquid film acting as the dominant thermal resistance to heat transfer.⁵¹ Meanwhile, the Cu tube with dropwise behavior showed improved performance over the filmwise tube ($\overline{U}_{\text{dropwise}} = 13.15$ \pm 0.73 kW/m² K) because as discrete droplets roll off the surface by gravity they also sweep other droplets to clean the surface for re-nucleation.9 The nanostructured CuO surface heat flux was highly dependent on the condensation mode



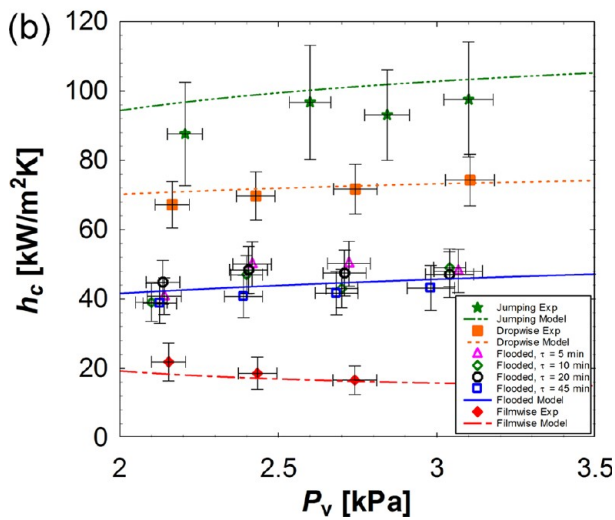


Figure 5. Heat transfer performance as a function of supersaturation and vapor pressure. (a) Experimental steady state log mean water to vapor temperature difference ($\Delta T_{\rm LMTD}$) as a function of overall surface heat flux (q'') for tube surfaces undergoing filmwise, dropwise, flooded, and jumping condensation (CuO chemical oxidation time $\tau = 10$ min, chamber vapor pressure $P_v = 2700 \pm 68$ Pa, $1.02 < S \le 1.6$). Rapid droplet removal due to coalescence induced droplet jumping results in the highest heat fluxes for the jumping sample (S < 1.12). However, flooding of the surface at higher heat fluxes results in rapid performance degradation and transition into the flooded condensation mode (S > 1.12). Data for the flooded sample at low supersaturations (S < 1.12, open triangles) were obtained by flooding the surface and decreasing $\Delta T_{\rm LMTD}$. Due to hysteresis, the jumping behavior was not recovered. (b) Experimental and theoretical steady state condensation coefficient (h_c) as a function of saturated vapor pressure (P_v) for tube surfaces undergoing filmwise, dropwise, flooded ($\tau = 5$, 10, 20, and 45 min), and jumping ($\tau = 10$ min) condensation (see Supporting Information, section S6). Jumping condensation shows the highest condensation HTC for low supersaturations (S < 1.12). Error bars indicate the propagation of error associated with the fluid inlet and outlet temperatures (± 0.2 K) and pressure measurement ($\pm 2.5\%$). The jumping surface error bars are the largest due to the relatively low heat fluxes measured $(q'' < 80 \text{ kW/m}^2)$, corresponding to the smaller fluid inlet to outlet temperature difference. The theoretical predictions (dotted lines) were obtained from the droplet growth and distribution model (for model derivation and parameters, see Supporting Information, section S7).

(jumping or flooded), as discussed previously. When the jumping droplet removal mechanism was favored (star symbols, S < 1.12, $\Delta T_{\rm LMTD} < 5$ K), the CuO tube showed the highest heat transfer performance ($\overline{U}_{\text{jumping}}$ = 16.5 \pm 2.20 kW/m² K), representing a 25% larger overall heat flux than the dropwise condensing surface. However, when the supersaturation increased to the point of flooding (empty and filled triangle symbols, S > 1.12), the heat transfer performance reduced below that of the dropwise Cu sample ($\overline{U}_{\text{flooded}} = 10.1 \pm 0.98$ kW/m² K) due to droplet pinning but remained above that of the filmwise sample. The significant performance hysteresis of the CuO surface allowed for heat transfer measurements to be obtained at low supersaturations (S < 1.12) for the flooded regime (empty triangle symbols) by first flooding the surface and then progressively increasing the cooling water temperature to reduce the supersaturation.

We also investigated the effect of vapor pressure (2 kPa $< P_{v}$ < 3.6 kPa) on the overall heat transfer performance to provide further insight into the condensation process on these surfaces, as well as to demonstrate the applicability of these surfaces for systems requiring different operating conditions. Figure 5b shows the steady state condensation HTC at the tube surface, h_{cl} as a function of the chamber vapor pressure, P_{vl} . First, to ensure the accuracy of our experimental results, we compared our baseline measurements to literature values, and showed that our measured filmwise and dropwise HTCs are in good agreement to those of Young et al. ($h_{\text{filmwise}} = 19 \pm 1.1 \text{ kW/m}^2$ $(K)^{52}$ and Marto et al. $(h_{dropwise} = 75 \pm 15 \text{ kW/m}^2 \text{ K})^{53}$ Accordingly, with the jumping condensation, we demonstrated a 30% higher HTC in comparison to dropwise condensation on the smooth Cu tube ($h_{\text{jumping}} = 92 \pm 12 \text{ kW/m}^2 \text{ K}$). Meanwhile, flooding of the surface at higher supersaturations led to a 40% degradation compared to dropwise condensation on the smooth Cu tube $(h_{\text{flooded}} = 44 \pm 6 \text{ kW/m}^2 \text{ K}).$

To explain the experimental results and investigate the heat transfer dependence on surface structure and vapor pressure, we used our developed model that incorporates thermalresistance-based droplet growth, the emergent droplet wetting morphology, and droplet distribution theory (see Supporting Information, section S7). The results from the model (lines) shown in Figure 5b are in excellent agreement with the experiments (symbols). For the jumping and flooded performance, the model results were obtained using experimentally determined droplet departure radii \hat{R} ($\hat{R}_{dropwise} \approx 1.3$ mm, $\hat{R}_{\text{jumping}} \approx 7 \, \mu\text{m}$, $\hat{R}_{\text{flooded}} \approx 2 \, \text{mm}$), contact angles, and a nucleation density N estimated based on previous ESEM studies of condensation on these CuO surfaces ($N_{\rm nanostructured} \approx$ $3N_{\rm smooth}$). The significant enhancement of the condensation heat transfer coefficient demonstrated with the jumping CuO surface, compared to the smooth dropwise and flooded CuO surfaces, is explained as follows. The increased number of smaller droplets maintains a smaller conduction resistance and ≈50% enhanced condensation heat transfer performance when compared to smooth dropwise condensing surfaces. 17,18 This result was obtained by incorporating the average steady state droplet size distribution for the jumping droplet surface, 2R =7.6 \pm 2.2 μ m (see Figure 2 and Supporting Information, section S5), into our model. In addition, the formation of the PW droplet morphology during condensation decreases the composite thermal resistance beneath the droplet, and together with the jumping removal mechanism further enhances the heat transfer. However, after flooding, the heat transfer degrades because the increased pinning force at the contact line of the

Wenzel droplets inhibits jumping and gravity is required to shed droplets from the surface. Accordingly, these droplets need to grow to sizes 2 orders of magnitude larger than in the jumping mode before being removed, leading to an increased population of large droplets which have a higher conduction thermal resistance and, consequently, reduce the heat transfer coefficient. The modeling results for the flooded sample show that the larger average droplet departure radius ($\hat{R}_{flooded} = 2$ mm) is primarily responsible for the ≈40% lower heat transfer performance when compared to the dropwise sample. However, there is also an additional effect associated with large pinned droplets at the bottom of the tube sample that effectively insulates up to 15% of the surface (Figure 3e), thus contributing to the performance discrepancy of the flooded sample compared to the dropwise sample. Finally, the jumping surface showed stronger pressure dependence, in both the model and experiment, when compared to the other surface types. This result is due to the fact that during individual droplet growth at small sizes $(R < 7 \mu m)$, the droplet conduction resistance is smaller than the interfacial mass transfer resistance. Accordingly, in the case of jumping surfaces, the majority of the condensing droplets sizes were small enough $(R < 7 \mu m)$ such that the interfacial mass transfer resistance, which is sensitive to vapor pressure,⁵¹ became comparable to the conduction resistance. Therefore, the heat transfer coefficient of the jumping surface varied more with vapor pressure than that of the other surfaces.

The outcomes of this work support the findings that both the droplet removal method (jumping versus gravitational shedding) and the emergent droplet morphology are critical in realizing enhanced condensation heat and mass transfer over state-of-the-art dropwise condensing surfaces. Furthermore, the experimental results suggest that nanostructured superhydrophobic surfaces have limitations for high heat flux applications due to progressive flooding of the surface and the formation of highly pinned liquid droplets. Although the presented results show the CuO nanostructure are ideal in terms of creating efficient droplet jumping and offer considerable heat transfer enhancement, the identified flooding mechanism presents a need for further reduction in the structure scale and/or reduction and control of the nucleation density at elevated supersaturations via engineering of the hydrophobic coating at length scales on the order of 10 nm or less. In addition, the CuO surfaces in this work present an opportunity to enhance condensation in the presence of noncondensable gases (NCGs) due to the potential for significant boundary layer mixing created by high-frequency droplet jumping. Much work has been done to show the importance of vapor flow and droplet shedding on condensation heat transfer enhancement in the presence of NCGs via boundary layer mixing. 48,55,56 These surfaces therefore promise opportunities for applications such as water harvesting, desalination or dehumidification, where the relative driving potential for condensation is low and NCGs are present.57

In summary, we experimentally demonstrated that, by using readily scalable nanostructured CuO surfaces, water condensation with droplet jumping can be achieved while minimizing the parasitic thermal resistances (oxide thickness). As a result, 25% higher overall heat flux and 30% higher condensation heat transfer coefficients compared to state-of-the-art dropwise condensing Cu surfaces were realized at low heat fluxes and, correspondingly, low supersaturations (S < 1.12). At high supersaturations (S > 1.12), flooding of the nanostructured

surfaces led to the formation of highly pinned Wenzel droplets, which degraded the condensation heat transfer coefficient by 40% compared to the smooth dropwise condensing tube. These results provide guidelines for the fabrication of high performance nanostructured CuO surfaces for low condensation heat flux applications. Furthermore, the results underscore the importance of the operating conditions for condensation heat and mass transfer on nanostructured superhydrophobic surfaces and also provide insights into the surface design requirements for high heat flux applications.

ASSOCIATED CONTENT

S Supporting Information

Five videos showing all condensation processes, as well as further information on data collection methodology, the experimental setup/procedure, and condensation modeling. This material is available free of charge via the Internet at http://pubs.acs.org.

AUTHOR INFORMATION

Corresponding Author

*E-mail: enwang@mit.edu.

Present Address

Thermal Management and Eco-sustainability Research Group, Bell Laboratories Ireland, Alcatel-Lucent, Blanchardstown Business and Technology Park, Snugborough Rd, Dublin 15, Ireland.

Notes

The authors declare no competing financial interest.

ACKNOWLEDGMENTS

We gratefully acknowledge funding support from the MIT S3TEC Center, an Energy Frontier Research Center funded by the Department of Energy, Office of Science, Office of Basic Energy Sciences. We also acknowledge the support from the National Science Foundation through the Major Research Instrumentation Grant for Rapid Response Research (MRI-RAPID) for the microgoniometer. This work was performed in part at the Center for Nanoscale Systems (CNS), a member of the National Nanotechnology Infrastructure Network (NNIN), which is supported by the National Science Foundation under NSF award no. ECS-0335765. CNS is part of Harvard University. R.E. acknowledges funding received from the Irish Research Council for Science, Engineering, and Technology, cofunded by Marie Curie Actions under FP7. Y.N. acknowledges funding received from Basic Science Research Program through the National Research Foundation of Korea (NRF) funded by the Ministry of Education, Science and Technology (No. 2012R1A1A1014845). N.M., R.E., Y.N., and E.N.W. conceived the initial idea of this research. E.N.W. guided the work. N.M., R.E., N.D., K.L., and J.S. carried out the experiments and collected data. N.M., R.E., and E.N.W. were responsible for writing the paper. N.M. carried out the theoretical analysis. N.M., K.L., and N.D. analyzed the data.

REFERENCES

- (1) Andrews, H. G.; Eccles, E. A.; Schofield, W. C. E.; Badyal, J. P. S. Three-Dimensional Hierarchical Structures for Fog Harvesting. *Langmuir* **2011**, 27, 3798–3802.
- (2) Milani, D.; Abbas, A.; Vassallo, A.; Chiesa, M.; Al Bakri, D. Evaluation of Using Thermoelectric Coolers in a Dehumidification System to Generate Freshwater From Ambient Air. *Chem. Eng. Sci.* **2011**, *66*, 2491–2501.

- (3) Khawaji, A. D.; Kutubkhanah, I. K.; Wie, J. M. Advances in seawater desalination technologies. *Desalination* **2008**, 221, 47–69.
- (4) Kim, M. H.; Bullard, C. W. Air-side performance of brazed aluminum heat exchangers under dehumidifying conditions. *Int. J. Refrig.* **2002**, *25*, 924–934.
- (5) Beer, J. M. High efficiency electric power generation: The environmental role. *Prog. Energy Combust.* **2007**, *33*, 107–134.
- (6) Perez-Lombard, L.; Ortiz, J.; Pout, C. A review on buildings energy consumption information. *Energy Buildings* **2008**, *40*, 394–398.
- (7) Li, B. Z.; Yao, R. M. Urbanisation and its impact on building energy consumption and efficiency in China. *Renewable Energy* **2009**, 34, 1994–1998.
- (8) Schmidt, E.; Schurig, W.; Sellschopp, W. Versuche über die Kondensation von Wasserdampf in Film- und Tropfenform. *Forsch. Ing.* **1930**, *1*, 53–63.
- (9) Rose, J. W. Dropwise condensation theory and experiment: a review. *Proc. Inst. Mech. Eng. A* **2002**, *216*, 115–128.
- (10) Rose, J. W. On the Mechanism of Dropwise Condensation. *Int. J. Heat Mass Transfer* **1967**, *10*, 755–762.
- (11) Kim, H. Y.; Lee, H. J.; Kang, B. H. Sliding of Liquid Drops Down an Inclined Solid Surface. *J. Colloid Interface Sci.* **2002**, 247, 372–380.
- (12) Dimitrakopoulos, P.; Higdon, J. J. L. On The Gravitational Displacement of Three-Dimensional Fluid Droplets From Inclined Solid Surfaces. *J. Fluid Mech.* **1999**, 395, 181–209.
- (13) Boreyko, J. B.; Chen, C. H. Self-Propelled Dropwise Condensate on Superhydrophobic Surfaces. *Phys. Rev. Lett.* **2009**, 103, 184501–184504.
- (14) Lafuma, A.; Quere, D. Superhydrophobic States. *Nat. Mater.* **2003**, *2*, 457–460.
- (15) Chen, X.; et al. Nanograssed Micropyramidal Architectures for Continuous Dropwise Condensation. *Adv. Funct. Mater.* **2011**, *21*, 4617–4623.
- (16) Dietz, C.; Rykaczewski, K.; Fedorov, A. G.; Joshi, Y. Visualization of Droplet Departure on a Superhydrophobic Surface and Implications to Heat Transfer Enhancement During Dropwise Condensation. *Appl. Phys. Lett.* **2010**, *97*, 033101–033104.
- (17) Enright, R.; Dou, N.; Miljkovic, N.; Nam, Y.; Wang, E. N. Condensation on Superhydrophobic Copper Oxide Nanostructures. 3rd Micro/Nanoscale Heat & Mass Transfer International Conference, Atlanta, GA, March 3–6, 2012.
- (18) Miljkovic, N.; Enright, R.; Wang, E. N. Effect of Droplet Morphology on Growth Dynamics and Heat Transfer during Condensation on Superhydrophobic Nanostructured Surfaces. *ACS Nano* **2012**, *6*, 1776–1785.
- (19) Rykaczewski, K.; et al. Three Dimensional Aspects of Droplet Coalescence During Dropwise Condensation on Superhydrophobic Surfaces. *Soft Matter* **2011**, *7*, 8749–8752.
- (20) Boreyko, J. B.; Zhao, Y. J.; Chen, C. H. Planar jumping-drop thermal diodes. *Appl. Phys. Lett.* **2011**, *99*, 234105–234107.
- (21) Enright, R.; Miljkovic, N.; Al-Obeidi, A.; Thompson, C. V.; Wang, E. N. Superhydrophobic Condensation: The Role of Length Scale and Energy Barriers. *Langmuir* **2012**, *40*, 14424–14432.
- (22) Miljkovic, N.; Enright, R.; Wang, E. N. Growth Dynamics During Dropwise Condensation on Nanostructured Superhydrophobic Surfaces. 3rd Micro/Nanoscale Heat & Mass Transfer International Conference, Atlanta, GA, March 3–6, 2012.
- (23) Narhe, R. D.; Khandkar, M. D.; Shelke, P. B.; Limaye, A. V.; Beysens, D. A. Condensation-Induced Jumping Water Drops. *Phys. Rev. E* **2009**, *80*, 031601–031605.
- (24) Rykaczewski, K. Microdroplet Growth Mechanism during Water Condensation on Superhydrophobic Surfaces. *Langmuir* **2012**, 28, 7720–7729.
- (25) Rykaczewski, K.; Scott, J. H. J. Methodology for Imaging Nanoto-Microscale Water Condensation Dynamics on Complex Nanostructures. ACS Nano 2011, 5, 5962—5968.
- (26) Rykaczewski, K.; et al. How nanorough is rough enough to make a surface superhydrophobic during water condensation? *Soft Matter* **2012**, *8*, 8786–8794.

(27) Liu, T. Q.; Sun, W.; Sun, X. Y.; Ai, H. R. Mechanism study of condensed drops jumping on super-hydrophobic surfaces. *Colloids Surf., A* **2012**, *414*, 366–374.

- (28) Kim, S.; Kim, K. J. Dropwise Condensation Modeling Suitable for Superhydrophobic Surfaces. *J. Heat Transfer* **2011**, *133*, 081501–081507.
- (29) Incropera, F. P.; DeWitt, D. P. Fundamentals of heat and mass transfer, 2nd ed.; Wiley: New York, 1985.
- (30) Kwak, K.; Kim, C. Viscosity and thermal conductivity of copper oxide nanofluid dispersed in ethylene glycol. *Korea-Aust. Rheol. J.* **2005**, 17, 35–40.
- (31) Cao, L. L.; Jones, A. K.; Sikka, V. K.; Wu, J. Z.; Gao, D. Anti-Icing Superhydrophobic Coatings. *Langmuir* **2009**, *25*, 12444–12448.
- (32) Gibbs, J. W.; Bumstead, H. A.; Van Name, R. G. The scientific papers of J. Willard Gibbs; Longmans, Green and Co.: New York, 1906.
- (33) Quere, D. Wetting and roughness. Annu. Rev. Mater. Res. 2008, 38, 71–99.
- (34) Nam, Y.; Ju, Y. S. A comparative study of the morphology and wetting characteristics of micro/nanostructured Cu surfaces for phase change heat transfer applications. *J. Adhes. Sci. Technol.* **2012**, 1–14.
- (35) Nam, Y.; Ju, Y. S. Comparative Study of Copper Oxidation Schemes and Their Effects on Surface Wettability. *Imece* 2008: Heat Transfer, Fluid Flows, Therm. Syst. 2009, 10 (Pts A–C), 1833–1838.
- (36) Nam, Y.; Sharratt, S.; Byon, C.; Kim, S. J.; Ju, Y. S. Fabrication and Characterization of the Capillary Performance of Superhydrophilic Cu Micropost Arrays. *J. Microelectromech. Syst.* **2010**, *19*, 581–588.
- (37) Fadeev, A. Y.; McCarthy, T. J. Self-Assembly Is Not the Only Reaction Possible between Alkyltrichlorosilanes and Surfaces: Monomolecular and Oligomeric Covalently Attached Layers of Dichloro- and Trichloroalkylsilanes on Silicon. *Langmuir* **2000**, *16*, 7268–7274.
- (38) Dietz, C.; Rykaczewski, K.; Fedorov, A.; Joshi, Y. ESEM Imaging of Condensation on a Nanostructured Superhydrophobic Surface. *J. Heat Transfer* **2010**, *132*, 080904.
- (39) Miljkovic, N.; Enright, R.; Maroo, S. C.; Cho, H. J.; Wang, E. N. Liquid Evaporation on Superhydrophobic and Superhydrophilic Nanostructured Surfaces. *J. Heat Transfer* **2011**, *133*, 080903.
- (40) Rykaczewski, K.; Scott, J. H. J.; Fedorov, A. G. Electron Beam Heating Effects During Environmental Scanning Electron Microscopy Imaging of Water Condensation on Superhydrophobic Surfaces. *Appl. Phys. Lett.* **2011**, *98*, 093101–093103.
- (41) Rykaczewski, K.; et al. Dynamics of Nanoparticle Self-Assembly into Superhydrophobic Liquid Marbles During Water Condensation. *ACS Nano* **2011**, *5*, 9746–9754.
- (42) Anand, S.; Son, S. Y. Sub-Micrometer Dropwise Condensation Under Superheated and Rarefied Vapor Condition. *Langmuir* **2010**, 26, 17100–17110.
- (43) Varanasi, K. K.; Deng, T. In 12th Ieee Intersociety Conference on Thermal and Thermomechanical Phenomena in Electronic Systems, Los Vegas, NV, 2010; pp 1–5.
- (44) Varanasi, K. K.; Hsu, M.; Bhate, N.; Yang, W. S.; Deng, T. Spatial Control in the Heterogeneous Nucleation of Water. *Appl. Phys. Lett.* **2009**, 95, 094101–094103.
- (45) Anderson, D. M.; et al. Using Amphiphilic Nanostructures To Enable Long-Range Ensemble Coalescence and Surface Rejuvenation in Dropwise Condensation. *ACS Nano* **2012**, *6*, 3262–3268.
- (46) Cheng, J.; Vandadi, A.; Chen, C. L. Condensation heat transfer on two-tier superhydrophobic surfaces. *Appl. Phys. Lett.* **2012**, *101*, 131901–131904.
- (47) Blanchette, F.; Bigioni, T. P. Partial coalescence of drops at liquid interfaces. *Nat. Phys.* **2006**, *2*, 254–257.
- (48) Ma, X. H.; Zhou, X. D.; Lan, Z.; Li, Y. M.; Zhang, Y. Condensation Heat Transfer Enhancement in the Presence of Non-Condensable Gas Using the Interfacial Effect of Dropwise Condensation. *Int. J. Heat Mass Transfer* **2008**, *51*, 1728–1737.
- (49) Vosough, A.; et al. Improvement Power Plant Efficiency with Condenser Pressure. *Int. J. Multidiscipl. Sci. Eng.* **2011**, *2*, 38–43.

(50) Bejan, A. Fundamentals of exergy analysis, entropy generation minimization, and the generation of flow architecture. *Int. J. Energy Res.* **2002**, *26*, 545–565.

- (51) Carey, V. P. Liquid-Vapor Phase-Change Phenomena: An Introduction to the Thermophysics of Vaporization and Condensation Processes in Heat Transfer Equipment, 2nd ed.; Taylor and Francis: London, 2008.
- (52) Young, E. H.; Briggs, D. E. The Condensing of Low Pressure Steam on Vertical Rows of Horizontal Copper and Titanium Tubes. *AIChE J.* **1966**, *12*, 31–35.
- (53) Marto, P. J.; Looney, D. J.; Rose, J. W.; Wanniarachchi, A. S. Evaluation of Organic Coatings for the Promotion of Dropwise Condensation of Steam. *Int. J. Heat Mass Transfer* **1986**, *29*, 1109–1117.
- (54) Miljkovic, N.; Enright, R.; Wang, E. N. Modeling and Optimization of Condensation Heat Transfer on Micro and Nanostructured Superhydrophobic Surfaces. *J. Heat Transfer* **2012**, in press.
- (55) Rose, J. W. Approximate equation for forced convection in the presence of non-condensable gas on flat plate and horizontal tube. *Int. J. Heat Mass Transfer* **1980**, 23, 539–546.
- (56) Maheshwari, N. K.; Saha, D.; Sinha, R. K.; Ritomi, M. Investigation oncondensation in presence of a noncondensable gas for a wide range of Reynolds number. *Nucl. Eng. Des.* **2004**, 227, 219–238.
- (57) Thiel, G. P.; Lienhard, J. H. Entropy generation in condensation in the presence of high concentrations of noncondensable gases. *Int. J. Heat Mass Transfer* **2012**, *55*, 5133–5147.